The Chemistry and Topography of Stabilized and Functionalized Graphene Oxide Coatings

Firas Awaja *[1, 2], Manoj Tripathi[3], Tsz-Ting Wong [4], Timothy O'Brien[2], Giorgio Speranza [5]

[1] Department of Orthopaedic Surgery, Medical University Innsbruck, Innrain 36, Innsbruck, Austria

[2] Regenerative Medicine Institute (REMEDI) and CÚRAM Centre for Research in Medical Devices, National University of Ireland, Galway, Ireland

[3] Department of Mathematics and Physical Sciences, University of Sussex, Brighton, UK

[4] Department of Mechanical Engineering, The Hong Kong Polytechnic University, Hong Kong

[5] Fondazione Bruno Kessler, Via Sumarrive 18, Trento, 38122, Italy

Abstract

GO thin films and coatings are regarded as superior in quality to other materials especially for biomedical applications. However, the lack of stability and understanding of their structure and defects hinder their use in value added applications. Here, we stabilized GO by reduction and functionalization through multiple plasma treatments with polymerizing (to deposit a crosslinking and compressing layer of diamond like carbon, DLC) and non-polymerizing precursors (H_2, O_2 and N_2). The hybrid GO and DLC coatings on semi crystalline PEEK (Polyether-ether-ketone) were evaluated using AFM, SEM and XPS. The GO deposited layer showed roughness around 70 nm and, despite care, resulted in several wrinkles and particle aggregations. The hybrid coatings conformed to the roughness and crystalline features of PEEK. XPS showed that the DLC layer cross-linked the GO nano-flakes while not completely masking which enable the partial exposure of GO. The GO-DLC hybrid interface is higher in thickness than the PEEK-GO and is dominating the overall thickness of the hybrid structure ≈ 13± 1 µm. XPS measurements showed that the often unstable C-O functional groups on the surface of the hybrid coating can be reduced by effective plasma treatment. Plasma treatments also generated C=O functional groups that probably originated from the decomposed carboxyl groups. The plasma

treatment also contributed to the reduction of GO. Treatment with H_2 was more effective in oxygen reduction than with the N_2, however, treatment with N_2 increased the reactants on GO as N_2 is heavier tending to deposit more on a surface. Plasma treatment with O_2 increased the surface oxygen content further and hence more defects on the hybrid surface.

Keywords

Graphene oxide; thin films; coatings; XPS; molecular structures; graphene

*Author for correspondence

Introduction

Graphene oxide (GO) and reduced graphene oxide (rGO), are oxide forms of graphene having the same monatomic structure and hexagonal carbon framework but with different physical and chemical properties [1, 2,]. These materials were extensively utilized in current research because of the superior properties and the possibility to produce bulk quantity by the exfoliation of graphite. However, GO contains a considerable amount of residual oxygen which is difficult to be removed leading to a large number of structural defects. Moreover, owing to the high polarity of GO surfaces, water molecules are easily coupled onto GO surfaces and penetrate through leading to detachment of GO flakes, therefore, the stability of GO substrates in aqueous environments is still questionable for bio-applications.

The carbon atoms in graphene are tightly packed together through the sp^2 orbital hybridization that is a combination of orbitals s, p_x and p_y constituting of the σ-bond and π-bond. Based on graphene structure, GO is non-stoichiometric, consisting of carbon sheet covalently bonded to oxygen-containing groups including epoxy (R-O-R') and hydroxyl (R-OH) groups at the basal plane and carbonyl (C=O), carboxyl (R-COOH) and lactol (O-C-O) functionalities at the edge[3-7]. The presence of these functional groups offer GO with several advantages, such as tunable electronic property through reduction process

changing GO from insulation to conduction[8], effective solution processability with solvents, hydrophilic characteristics, making GO ready to attract water molecules for stabilization, anti-restacking ability of the carbon sheets, and anchoring ability providing reactive sites to immobilize various active species over GO sheets[9]. On the contrary, the oxygen functional groups in GO could degrades the thermal, electrical and mechanical properties relative to graphene [3, 4, 6, 10-12]. The presence of oxygenic moieties causes thermal decomposition of GO at the temperature between 150-200 °C leading to the evolution of CO and CO_2[7]]. During low temperature reduction of GO, the water molecules trapped among the layers are desorbed first in the RT – 100 0C temperature range. From 100 0C to 150 0C, hydroxyl and epoxy bonds are gradually decomposed. Concurrently, carbonyl and sp2 bonds are formed [13]. Carbonyl bonds will be then degraded at higher temperatures and hence make it the most thermally stable bond.

The mechanical properties of GO are mostly related to the physical and structural properties that are the thickness and oxidation degree (the ratio of carbon to oxygen) [14, 15], therefore, the Young's modulus and tensile strength have been reported in a wide range of 6-42GPa and 76-293MPa respectively[16-20]. Structural defects, intrinsic type (sp^2-type) and extrinsic type (vacancy-type), identified in the graphitic structures of GO and rGO [16-18] are the critical determinants for the physical properties. Compton [3] summarized the works done on GO and rGO regarding the production methods with manipulating GO including the synthesis of transparent conductive thin films, their properties, and applications. Banhart [16] reviewed the defects types, generations, and properties of graphene and stated the electronic and optical properties of graphene can be manipulated by managing the intrinsic or extrinsic type defects. It is worth noting that the contained residual oxygen and other heteroatoms in GO and rGO degrades the mechanical strength of defect-free structures as extrinsic type defects[3]. Extrinsic defects also deviate the properties like electrical conductivity of graphite and rGO from defect-free structures, nevertheless,

Dreyer and Mao [4, 6] found these defects serve as active sites for reduction-oxidation (redox) reactions. The restoration strategy could be utilized by supplying additional carbon atoms on GO, which reduces the chemical functional groups attached to the carbon atoms and inhibits the sp^2-interactions, was found to repair the defective graphitic structure thus improve the stability. In this respect, partial and complete reduction methods of GO including the graphitization at high temperature[21, 22], epitaxial growth[23], charge-transfer chemical doping[24], plasma deposition[25], and chemical vapour deposition (CVD) [26] have been extensively studied in detail[27, 28].

The stability of GO membranes in water is rather in debate still. Yeh [29] showed that GO instability is due to the electrostatic repulsion of negatively charged GO sheets on hydration. Another study showed the stability of GO is not affected by the pH (4-10 value) of the solution, but the salt type and ionic strength have significant influences under the electrostatic layer-to-layer compression[30]. The stability of GO powdered sheets in aqueous solution can be enhanced by converting them into membrane form with few micron thickness through filtering and drying procedures[31]. While the stability of GO membranes is achieved through the crosslinking of individual GO sheets with the implementation of multivalent cationic metal contaminants[29]. Carbonaceous nanomaterials of good conductivity, chemical stability and large surface area enhances the charge storage through generating electric double layer capacitors by adsorption of ions. Another possibility is by forming a pseudo capacitor and producing energy from redox reaction during charge/discharge [32, 33]. Accordingly, the intercalation of molecules like carbon nanotube (CNT) and fullerene is useful for charge storage applications by electrostatic adsorption of ions [33].

Previous studies showed GO membranes exhibit hydration or solvation properties which is not found in their precursor GO powders [34] and GO membranes show a faster water permeation and decreased permeability for alcohols like methanol and ethanol[35, 36]. Moreover, GO membranes permeated NaOH faster than Na salts indicating their expansion in alkaline solutions [37] and GO membranes emerged as

efficient filters for molecular or ionic separation[35]. Chowdhury also observed the stability of GO in natural aquatic environment and indicated aqueous transportation of GO is possible and useful for effluent treatment. Hence, all the findings mentioned confirm the stability of GO is directly correlated to the carbon-to-oxygen ratio in GO sheets and their cross linkages among the GO sheets.

Polyether-ether-ketone (PEEK), a semi-crystalline thermoplastic with non-toxicity, natural radiolucency, excellent thermal and chemical stability, and good mechanical properties. PEEK have been a substitute for metal alloys in orthopedic applications[38-42]. However being bio-inert and hydrophobic limits its applications. Implementing diamond-like carbon (DLC) coatings on PEEK is a promising strategy for bio-applications owing to their good bio-compatibility, such as their elastic modulus close to the cortical bone in human, excellent tribological and mechanical properties[43-45]. However, the adhesive strength at the interface of DLC coating and PEEK substrate poses a weakness in performing the function when high internal compressive stress and corrosive environment are present in human body. Escudeiro and Dufils [43, 44] proposed incorporating with metallic compounds at the interlayers and altering the C to H ratio of the deposited thin film to improve the device performances. Bzaka *et al.*[46] explained that plasma assisted techniques as suitable option for controlled modification of a variety of biocompatible surfaces by surface oxidation, nitration, hydrolyzation and amination. Plasma treatment were shown to be effective method to decontaminate and sterilization of biomaterials and medically-relevant devices by generating active surfaces of plasma generated radicals. Moreover, desirable chemistry can be obtained by surface functionalization with specific moiety like amines, hydrogen, oxygen etc. which leads to controlled morphology, desirable substrate adhesion and stability.

The use of plasma treatments with graphene based materials provides an effective means of doping, generation of reactive species and other ionic parameters which modulates the charge transfer characteristics[47]. For instance, NH_3 plasma can induce nitrogen radical covalently binding with carbon

lattice, oxygen plasma treatment can alter the bandgap of graphene based materials, driving transition from semi-metallic to semiconductor [48]. Conversely, certain optimized plasma treatment at controlled atmosphere (eg. Remote methane plasma) used to reduce GO by lowering its oxygenic content and decreases band gap of the material. Furthermore, plasma-treatments enabled the reduction of GO to graphene that is facilitated by significant defect healing which causes improvement in material quality [25]. Thus, oxidation and reduction reaction carried out by controlled and optimized plasma treatment can regulate defects and functional groups which is useful for enabling life cycle of carbon based precursor. The present study employs plasma deposition to modify the surface of GO coated PEEK with DLC and implements SEM, AFM and XPS to evaluate the topography and chemical compositions of the DLC/GO solid thin film on PEEK. This engineered material is expected to achieve good stability in an aqueous environment, excellent tribological properties, and electrical characteristics for bio-applications.

Materials and Methods

Materials

Commercial graphene oxide (GO), dispersion (4mg/ml) in water obtained from Graphenea (Spain), was initially ultrasonicated at 40-50 °C for 2 hours. About 2-3ml of dispersed GO in water was drop-casted over polyether-ether-ketone (PEEK) polymer and dried at room temperature for 24 hours to produce GO/PEEK. PEEK substrates were then introduced in a plasma-enhanced chemical vapour deposition (PECVD) reactor for the deposition of diamond-like carbon (DLC) films to stabilize the GO coating.

PEEK Surface Modification

The plasma treatment apparatus that was used for this study was a custom build instrument. The plasma source is a COPRA GTE200 RF-inductively coupled plasma high density source from CCR-technology

GmbH, Germany supplied with a radiofrequency at 13.56 MHz and operated at 200W. In the deposition process, the pressure inside the reactor was maintained constantly at 0.15 mbar by adjusting a butterfly valve. Different plasma precursor mixtures shown in **Table 1** were utilized to obtain the DLC films deposited on GO with different chemical compositions and functional groups on their surfaces. Three groups of samples were produced for the study including plasma treated and deposited PEEK substrates (samples 1a-1f), the same plasma treatment adopted on GO-coated PEEK substrates (samples 2a-2f), and oxygen-rich precursors plasma treatment samples employed on GO-coated PEEK substrates (samples 3a and 3b). Pure methane (CH_4) and a mixtures of methane and hydrogen (CH_4+H_2) were utilized to deposit neutral DLC films, the mixture of methane and oxygen (CH_4+O_2) was utilized to introduce negative carboxyl and hydroxyl functional groups while the mixture of methane and nitrogen (CH_4+N_2) was utilized to deposit amine-rich coatings.

Table 1 Plasma precursor mixtures (in sccm) utilized for the deposition of DLC film on each sample

Samples	**Simple PEEK substrates**			
	CH_4	**H_2**	**O_2**	**N_2**
1a	80	0	0	0
1b	60	20	0	0
1c	54	26	0	0
1d	40	40	0	0
1e	30	30	20	0
1f	30	30	0	20
	GO/PEEK substrates			
	CH_4	**H_2**	**O_2**	**N_2**
2a	80	0	0	0
2b	60	20	0	0
2c	54	26	0	0
2d	40	40	0	0
2e	30	30	20	0
2f	30	30	0	20
	O^2-rich films on GO/PEEK substrates			
	CH_4	**H_2**	**O_2**	**N_2**
3a	40	0	40	0

3b	60	0	20	0

XPS Characterization

The surfaces of all samples were characterized using X-ray photoelectron spectroscopy (XPS), a non-destructive technique, to obtain their profiles of chemical composition, elemental concentration, and atoms bonding mechanisms. XPS analyses were performed using an Axis Ultra DLD from Kratos, UK equipped with a monochromated Al Kα radiation and 300µm x 700µm sample area. Charge compensation was employed due to the non-conductive substrates. The charge neutralizer in the instrument is coaxial to the analyzed lenses allowing optimal charge compensation even in the presence of surface roughness. A wide and high energy resolved spectrum was acquired for each sample. The final energy resolution was approximately 0.35eV in the last operating mode.

SEM

Scanning electron microscopy (SEM) was conducted using Jeol JSM7401F at 5KeV beam energy and 10 µA of emitted current. The SEM micrograph was carried out over PEEK substrate covered with GO, DLC and GO/DLC.

AFM

High resolution topography and roughness measurement was carried out by Psolver 47 NT-MDT in semi-contact mode. Silicon probe (stiffness nearly 30 N/m) radii approx. 10 nm has been used for imaging the samples in air conditions.

Results and Discussion

Topographic analysis from SEM and AFM measurement

Figure 1 is showing the topographic images from the SEM and AFM for different coatings namely DLC, GO and the hybrid structure of GO/DLC on the PEEK substrates. The GO has introduced the wrinkled structure (nealy 15 nm altitude) over the semi-crystalline PEEK morphology along with aggregated flakes. The DLC coatings conform the PEEK substrate (**Figure 1(b))** revealing comparable values of roughness (rms, root mean square) in **Table 2**. The GO layers elevated in altitude at the local nucleate site of the PEEK substrate that remarkably increases the roughness up to 3 folds. Unlike DLC, the distribution of GO flakes are not uniform and the interlayer spacing between GO-layers has contributed to the increase in roughness (**Figure 1(a, d**)). Deposition of DLC over wrinkled and accumulated GO surface further enhances the roughness of the hybrid structure (PEEK+GO+DLC) up to 4 folds. The improper conformation between DLC and GO at the wrinkled region is responsible for such higher roughness.

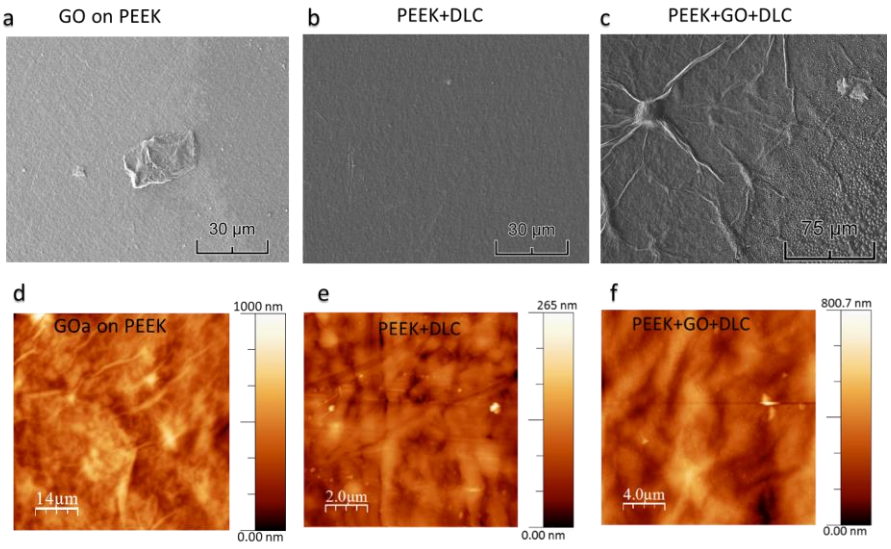

Figure 1 SEM micrograph of (a) PEEK covered GO showing contrast between GO layers, flakes and PEEK substrate; (b) uniform coverage of DLC on PEEK substrate; and (c) GO sandwiched between DLC and PEEK substrate with relatively high magnitude of wrinkle. AFM topographic image of (d)

thin GO coating with PEEK substrate; (e) DLC conformed with PEEK substrate; and (f) GO sandwiched between DLC and PEEK substrate.

Table 2 Roughness measurement in root mean square (rms) and average roughness (Ra)

Roughness	RMS (nm)
PEEK	22±2
PEEK+DLC	22±4
PEEK+GO	70±5
PEEK+GO+DLC	86±6

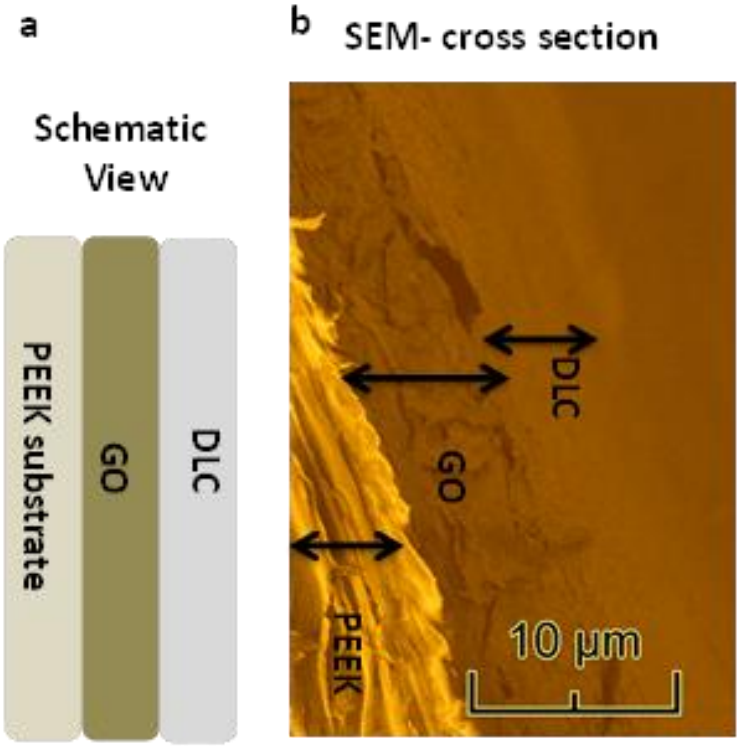

Figure 2 (a) Schematic view for the arrangement of GO and DLC layers over PEEK substrate. (b) SEM image of the cross section of the hybrid GO/DLC on the PEEK substrate. The arrows are showing the thickness of the corresponding layers. The present image is from sample no. 2d

The thickness and distribution of the GO/DLC over a PEEK substrate is clearly resolved in the cross-section area of the hybrid structure at **Figure 2**. Schematic view (**Figure 2(a)**) is showing the arrangement of the heterostructural coatings in which GO is sandwitched between PEEK and DLC. Cross-section SEM micrograph in **Figure 2(b)** is illustrating two major contrast from the interfaces (a) PEEK-GO and (b) GO-DLC. The sandwitched structure of GO is showing thickness of 8 microns due to compression from the DLC layer of thickness 4 microns. The interlayer separation between GO-DLC interface is higher than the PEEK-GO and is dominating overall thickness of the hybrid structure ≈ 13± 1 μm. The presence of interfacial gap between the DLC and GO indicates lower interfacial interaction between chemically inert DLC and GO rather than plasma enhanced PEEK-GO. While, PEEK-GO interface, the π-conjugated structure in the GO-graphitic basal plain can form strong π-π stacking interaction with the π-conjugated system (such as benzene ring) in PEEK[49]. The functional groups associated with GO can be used to bind heterostructures for higher mechanical, thermal and chemical stability[50, 51]. Peng et al. [49]found the improvement in thermal stability and mechanical properties at PEEK-GO interface due to π-conjugated structure. It helps to transfer the stress directly from the matrix to GO and stabilize the entire system. The interface between GO-DLC comprises functional groups of -OH, -COOH, -O- bonding to produced hydrogen bonds[52].

XPS

The elemental abundances of the plasma treated samples are summarized in **Table 3**. The carbon concentration is higher in the list of samples from 1a to 1f obtained from the plasma treatment on simple PEEK. The oxygen concentration is higher in the list of samples from 2a to 2f obtained from the plasma treatment on GO/PEEK. This implies the stabilizing films deposited on GO are unable to mask a high concentration of oxygen deriving from GO. The stabilization of GO is highly desired for the

substrates by which plasma treatment enables a much higher stability on the treated samples while preserves the functions of the underlying GO coating.

The stability of the GO films depends on the oxygen concentration present on the graphene flakes. Oxygen defects leads to a change of the carbon hybridization from sp^2 to sp^3 preventing π-π interaction. It is then expected that the higher is the oxygen content the lower is the coupling between flakes with decreased mechanical properties and stability. Smaller interaction between graphene sheets can also lead to risk of detachment with adverse consequences on its use. A diamond like amorphous hydrogenated films was deposited on the GO film to increase its solidity. The plasma deposition is performed that was generated using mixture of CH_4, H_2, O_2 and N_2 in different proportion. A high concentration of ions of the precursor molecules will readily react with the carbon atoms of the graphene flakes leading to the formation of an amorphous network steadily "gluing" the GO flake to flake.

The concentration of the oxygen and nitrogen, listed in **Table 3**, increases in both group of samples from 1a to 1f and 2a to 2f when O_2 and N_2 are introduced in the precursor mixtures respectively and surprisingly the higher oxygen concentration is obtained through N_3 treatment. The XPS results obtained from Bertoti [53] studying the surface composition of graphene and graphite treated by nitrogen plasma show agreeable results with the current study on GO which the oxygen and nitrogen concentration in the samples appear consistent against the carbon concentration. There are two processes can explain the results. When NH_3 with highly hydrophilic property is introduced in the reactor chamber, NH_3 fragments easily and couples with water molecules which are desorbed by the reactor walls and then deposited on the substrate surface. On the other hand, NH_3 fragmentation leads to the presence of hydrogen radicals which etches the substrate surface and unmask the underlying GO coating.

In **Figure 3A** the C1s core lines form pristine GO and PEEK together with the same polymer treated in plasma containing CH_4, O_2 and N_2 are shown. As it can be seen, in the C1s from GO the highest component is the one relative to the C-OH bonds. In pure PEEK this component is replicated but with a much less extent. The PEEK sample treated with pure CH_4 shows a carbon peak featured essentially by CH_x components. Only a mild asymmetry on the high BE side reveals the presence of weak oxidized components. Differently, the O_2 plasma treated PEEK shows a distinct C-OH component slightly higher respect to that of PEEK, and those related to carbonyl and carboxyl functional groups. Finally, the N_2 containing plasma treatment shows a less structured C1s peak since the -C-N- bonds fall at ~285.7eV rather near to the hydrocarbon CH_x main peak. Noticeable also difference among samples is the presence of the graphitic component only in the GO sample while in the other samples this peak is substituted by the hydrocarbon peak at 285eV.

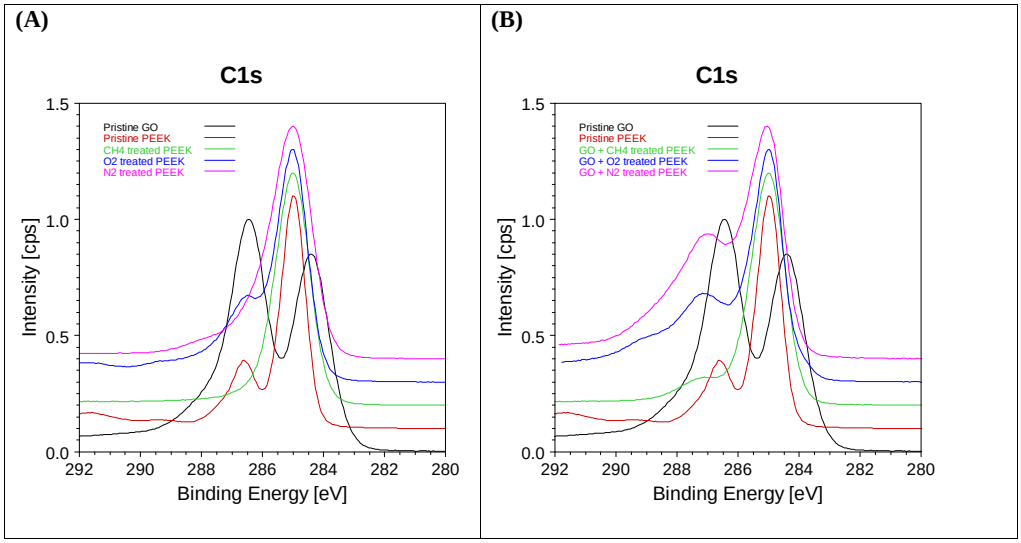

Figure 3: (A) C1s core lines from plasma treated PEEK samples. Spectra are normalized to a common height and shifted in ordinate to facilitate the comparison; (B) C1s core lines from GO + plasma treated

PEEK samples. Spectra are normalized to a common height and shifted in ordinate to facilitate the comparison.

Looking at values summarized in **Table 4**, it appears that the concentration of nitrogen based functional groups is significant only when N_2 is present as a plasma precursor. Difference is the case of the presence of graphene on the PEEK substrate. In this case, nitrogen is present in all the plasma treatments.

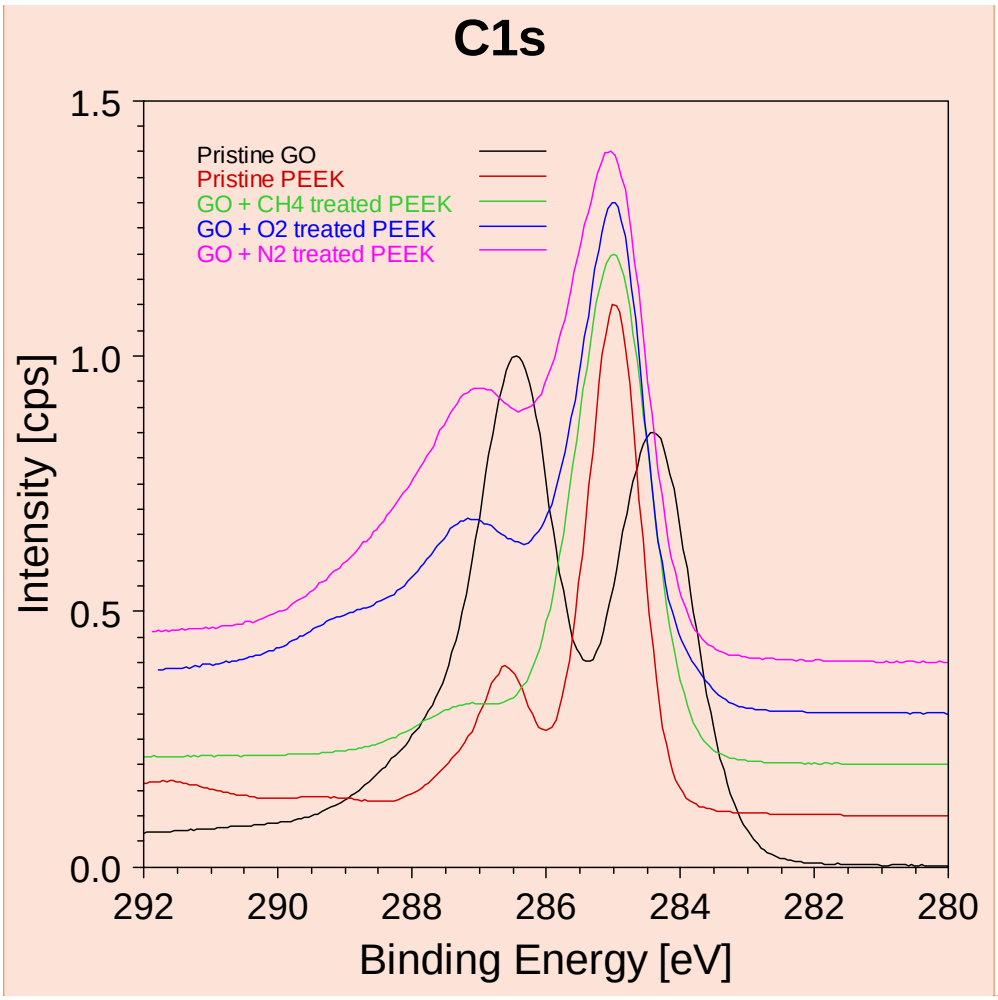

Figure 4 C1s core lines form the indicated samples. Spectra are normalized to a common height and shifted in ordinate to facilitate the comparison.

Figure 4 compares the C1s peaks of pristine GO and PEEK samples with those obtained after deposition of GO and subsequent plasma treatment only with CH_4, adding O_2 to the precursors or adding N_2. In this case we observe that already the sample treated with pure CH_4 displays oxidized components mainly described by C-OH functional groups. Similar to the work done by Baraket[54], a

Commented [mT1]: I think Giorgio forgot to delete the figure . It is similar to fig. 3 (B).

strong reduction in the O concentration in GO with a significant reduction on C-O was demonstrated effectively by introducing CH_4 plasma. The work also suggests the presence of carbon species plays a key role in increasing the sp^2 phase in GO upon reduction. From table 4 one sees that the CHx component increases. This is not the C-C graphitic sp2 component but likely carbon atoms as in polypropylene (sp3) which is described by fits a component at 285eV. Aromatic rings as benzene fall at 284.5eV which is not our case.

This components increase with O_2 containing plasma treatments. In particular in this case the carboxyl component become evident and this may play an important role in the cell assays because it is a polar component. Several reports showed that surface rich in oxygenic functional groups like hydroxy and carboxyl on a polymer surfaces and functionalized carbon materials (like graphene, GO and rGO) effectively inhibit the growth of bacteria like *E. coli* and *P. aeruginosa* by damaging the cell membrane especially at the edge region (rich in hydroxyl and carboxyl groups) [55, 56]. The respiratory proteins on the surface of bacteria behave as n-type semiconductors and electrons are effectively transferred from the microbial membrane to the carbon materials coated on a conducting surface responsible for retarding bacterial growth. By conducting direct contact between Gram-negative and Gram-positive bacteria to GO, a charge transfer between the bacteria and the carbon material responsible for microbial toxicity [55]. Thus, the presence of the oxygenic functional groups are characterized by biocidal and antifouling activities.

The XPS analyses from Zhao [57] yet well confirms our results which the O_2 plasma treatment on GO reduced the graphitic structure C=C-C while increased the other carbon-oxygen structures, C-OH, C=O and O-C=O. This implies O_2 plasma introduces numerous defects in GO providing more binding sites for molecule attachment. Finally, the sample treated with a plasma containing N_2 the C1s spectrum is

dominated by the CH_x component. At higher BE **Figure 4** shows the presence of a broad tail. This feature can be assigned to multiple bonds of carbon with nitrogen and with the different bonds with oxygen. Another similar study using XPS to analyse the composition and chemical state of GO treated by H_2 plasma and a gas mixture of H_2 and N_2 was done by Chen[58]. Various identified carbon-oxygen bonds, C-O in C-OH, epoxy type C-O-C, carbonyl type C=O, and carboxylic type O-(C=O), are similar to our results. The work also suggests C-O is unstable which can be reduced by effective plasma treatment. C=O is developed most probably from the decomposed carboxyl groups due to the plasma treatments. In terms of reducing GO, H_2 shows more effective than with the N_2 introduced, but on the other hand, implementing N_2 increases the reactants on GO as N_2 is heavier tending to deposit on a surface.

The behavior of the C1s associated to the different samples mirrors the concentration of the functional groups listed in **Table 4**. Peak fitting the core lines pertaining each of the samples it is possible to estimate the abundance of functional groups present on the substrate surface. These abundances will play an important role in the process of the cell adhesion and growth.

Table 3 Elemental abundance (in percent) estimated through XPS of the plasma treated sample surfaces

Samples	Simple PEEK substrates		
	C	**O**	**N**
1a	96.6	3.3	0.1
1b	97.2	2.7	0.1
1c	95.4	4.5	0.2
1d	93.8	5.7	0.5
1e	79.6	20.2	0.2
1f	87.4	6.5	6.1
	GO/PEEK substrates		
	C	**O**	**N**
2a	80.9	15.6	3.4
2b	74.3	20.8	4 9
2c	69.3	25.1	5.5

2d	81.6	15.7	2.7
2e	66.6	29.5	3.9
2f	58.6	32.2	9.2

Table 4 Abundance (in percent) of functional groups found on the substrate surfaces in relation to the performed plasma treatment

Samples	**Simple PEEK substrates**									
	C1s					**O1s**			**N1s**	
	Ar+CHx	**C-NH2**	**C-O-C**	**C=O**	**O-C=O**	**C=O**	**C-O**	**O-C-O**	**C-NH2**	**C-NH2+**
1a	86.89	0.06	6.7	2.12	0.86	0.74	1.84	0.72	0.04	0.03
1b	87.89	0.19	6.03	2.13	0.96	0.54	1.64	0.48	0.09	0.6
1c	82.01	1.06	8.6	2.6	1.12	0.83	2.69	0.91	0.08	0.07
1d	79.73	1.03	9.42	2.53	1.09	1.4	3.43	0.91	0.18	0.2
1e	51.2	0.64	19.25	5.28	3.21	6.71	12.6	0.84	0.06	0.16
1f	64.83	6.01	11.32	3.2	2.03	1.34	4.07	1.06	3.16	2.99
	GO/PEEK substrates									
	C1s					**O1s**			**N1s**	
	Ar+CHx	**C-NH2**	**C-O-C**	**C=O**	**O-C=O**	**C=O**	**C-O**	**O-C-O**	**C-NH2**	**C-NH2+**
2a	65.29	4.6	5.84	4.15	1.02	10.5	4.28	0.73	0.37	3.19
2b	54.96	4.26	8.16	5.84	1.1	13.6	5.94	1.24	0.55	4.3
2c	42.25	5.58	13.67	5.94	1.9	15.1	8.58	1.37	0.62	4.9
2d	59.95	3.89	9.79	6.25	1.77	10.3	4.59	0.73	0.37	2.33
2e	33.59	4.4	8.05	11.7	6.86	12.2	11.6	5.6	1.15	2.77
2f	25.17	10.4	16.61	6.31	2.04	14.6	11.1	6.43	5.52	3.65

Conclusion

The plasma deposition of DLC layer over GO coating created a stable hybrid coating through the actions of crosslinking and compression. XPS showed that plasma treatment enables a much higher stability on the treated samples while preserves the functions of the underlying GO coating. The deposited GO layer on PEEK took the shape of the local nucleate site of the PEEK substrate with remarkable increase in roughness up to 3 folds. Despite care, the distribution of GO flakes were not uniform with observable interlayer spacing that contributed to the increase in roughness. Deposition of

DLC over wrinkled and aggregated GO surface further increased the roughness of the hybrid structure up to 4 folds. The conformation of the DLC and associated plasma bombardment on the wrinkled GO region is responsible for such higher roughness. Effective plasma treatment lead to the reduction of the C-O functional groups on the coating surfaces which increased the coatings stability. XPS measurements showed that the oxygen reduction on the surface of the GO-DLC hybrid was possible using H_2 as a precursor. Using N_2 plasma treatment increased surface functionality while the use of O_2 oxidised the surface even further leading to increased defects. While the use of the plasma treatment post GO drop casting on PEEK improved stability and connectivity of the nano particles to each other and to PEEK. It would be beneficial development for this technology to plasma treat the PEEK surface prior to GO drop casting which may reduce the effects of wrinkling and agglomeration of the GO nano particles.

Acknowledgement

This publication has emanated from research conducted with the financial support of Science Foundation Ireland (SFI) and is co-funded under the European Regional Development Fund under Grant Number 13/RC/2073. This project has received funding from the European Union's Horizon 2020 research and innovation programme under the Marie Skłodowska-Curie grant agreement No 713690. FA would also acknowledge funding from the FWF under the Lise Meitner program (M-1777).

References

1. F. Bonaccorso, A. Lombardo, T. Hasan, Z. Sun, L. Colombo and A. C. Ferrari, *Materials today*, **2012**, 15, 564-589.
2. Y. Xu, H. Bai, G. Lu, C. Li and G. Shi, *Journal of the American Chemical Society*, **2008**, 130, 5856-5857.

3. O. C. Compton and S. T. Nguyen, *small*, **2010**, 6, 711-723.
4. D. R. Dreyer, S. Park, C. W. Bielawski and R. S. Ruoff, *Chemical Society Reviews*, **2010**, 39, 228-240.
5. W. Gao, L. B. Alemany, L. Ci and P. M. Ajayan, *Nature chemistry*, **2009**, 1, 403-408.
6. S. Mao, H. Pu and J. Chen, *Rsc Advances*, **2012**, 2, 2643-2662.
7. Q. Pan, C.-C. Chung, N. He, J. L. Jones and W. Gao, *The Journal of Physical Chemistry C*, **2016**, 120, 14984-14990.
8. H. A. Becerril, J. Mao, Z. Liu, R. M. Stoltenberg, Z. Bao and Y. Chen, *ACS nano*, **2008**, 2, 463-470.
9. F. Li, X. Jiang, J. Zhao and S. Zhang, *Nano energy*, **2015**, 16, 488-515.
10. V. Palermo, I. A. Kinloch, S. Ligi and N. M. Pugno, *Advanced Materials*, **2016**, 28, 6232-6238.
11. H. C. Schniepp, J.-L. Li, M. J. McAllister, H. Sai, M. Herrera-Alonso, D. H. Adamson, R. K. Prud'homme, R. Car, D. A. Saville and I. A. Aksay, *The Journal of Physical Chemistry B*, **2006**, 110, 8535-8539.
12. S. Stankovich, D. A. Dikin, R. D. Piner, K. A. Kohlhaas, A. Kleinhammes, Y. Jia, Y. Wu, S. T. Nguyen and R. S. Ruoff, *carbon*, **2007**, 45, 1558-1565.
13. E. Tegou, G. Pseiropoulos, M. Filippidou and S. Chatzandroulis, *Microelectronic Engineering*, **2016**, 159, 146-150.
14. H. Chen, M. B. Müller, K. J. Gilmore, G. G. Wallace and D. Li, *Advanced Materials*, **2008**, 20, 3557-3561.
15. L. Liu, J. Zhang, J. Zhao and F. Liu, *Nanoscale*, **2012**, 4, 5910-5916.
16. F. Banhart, J. Kotakoski and A. V. Krasheninnikov, *ACS nano*, **2010**, 5, 26-41.
17. S. Eigler, C. Dotzer and A. Hirsch, *Carbon*, **2012**, 50, 3666-3673.
18. K. Erickson, R. Erni, Z. Lee, N. Alem, W. Gannett and A. Zettl, *Advanced Materials*, **2010**, 22, 4467-4472.
19. Y. Gao, L.-Q. Liu, S.-Z. Zu, K. Peng, D. Zhou, B.-H. Han and Z. Zhang, *ACS nano*, **2011**, 5, 2134-2141.
20. J. Zhao, L. Liu and F. Li, *Graphene oxide: physics and applications*, Springer, 2015.
21. R. Rozada, J. I. Paredes, S. Villar-Rodil, A. Martínez-Alonso and J. M. Tascón, *Nano Research*, **2013**, 6, 216-233.
22. C.-Y. Su, Y. Xu, W. Zhang, J. Zhao, A. Liu, X. Tang, C.-H. Tsai, Y. Huang and L.-J. Li, *Acs Nano*, **2010**, 4, 5285-5292.
23. C. Berger, Z. Song, X. Li, X. Wu, N. Brown, C. Naud, D. Mayou, T. Li, J. Hass and A. N. Marchenkov, *Science*, **2006**, 312, 1191-1196.
24. Y. S. Yun, G. Yoon, M. Park, S. Y. Cho, H.-D. Lim, H. Kim, Y. W. Park, B. H. Kim, K. Kang and H.-J. Jin, *NPG Asia Materials*, **2016**, 8, e338.
25. M. Cheng, R. Yang, L. Zhang, Z. Shi, W. Yang, D. Wang, G. Xie, D. Shi and G. Zhang, *Carbon*, **2012**, 50, 2581-2587.
26. K. S. Kim, Y. Zhao, H. Jang, S. Y. Lee, J. M. Kim, K. S. Kim, J.-H. Ahn, P. Kim, J.-Y. Choi and B. H. Hong, *nature*, **2009**, 457, 706.
27. C. K. Chua and M. Pumera, *Chemical Society Reviews*, **2014**, 43, 291-312.
28. S. Pei and H.-M. Cheng, *Carbon*, **2012**, 50, 3210-3228.
29. C.-N. Yeh, K. Raidongia, J. Shao, Q.-H. Yang and J. Huang, *Nature chemistry*, **2015**, 7, 166.
30. I. Chowdhury, M. C. Duch, N. D. Mansukhani, M. C. Hersam and D. Bouchard, *Environmental science & technology*, **2013**, 47, 6288-6296.
31. D. A. Dikin, S. Stankovich, E. J. Zimney, R. D. Piner, G. H. Dommett, G. Evmenenko, S. T. Nguyen and R. S. Ruoff, *Nature*, **2007**, 448, 457.

32. J. Liu, A. G. Rinzler, H. Dai, J. H. Hafner, R. K. Bradley, P. J. Boul, A. Lu, T. Iverson, K. Shelimov and C. B. Huffman, *Science*, **1998**, 280, 1253-1256.
33. Q. Yang, S.-K. Pang and K.-C. Yung, *Journal of Power Sources*, **2016**, 311, 144-152.
34. A. Klechikov, J. Yu, D. Thomas, T. Sharifi and A. V. Talyzin, *Nanoscale*, **2015**, 7, 15374-15384.
35. J. Abraham, K. S. Vasu, C. D. Williams, K. Gopinadhan, Y. Su, C. T. Cherian, J. Dix, E. Prestat, S. J. Haigh and I. V. Grigorieva, *Nature nanotechnology*, **2017**, 12, 546-550.
36. M. Krueger, S. Berg, D. A. Stone, E. Strelcov, D. A. Dikin, J. Kim, L. J. Cote, J. Huang and A. Kolmakov, *ACS nano*, **2011**, 5, 10047-10054.
37. P. Sun, M. Zhu, K. Wang, M. Zhong, J. Wei, D. Wu, Z. Xu and H. Zhu, *Acs Nano*, **2012**, 7, 428-437.
38. L. Eschbach, *Injury*, **2000**, 31, D22-D27.
39. A. Godara, D. Raabe and S. Green, *Acta Biomaterialia*, **2007**, 3, 209-220.
40. A. Katzer, H. Marquardt, J. Westendorf, J. Wening and G. Von Foerster, *Biomaterials*, **2002**, 23, 1749-1759.
41. S. M. Kurtz and J. N. Devine, *Biomaterials*, **2007**, 28, 4845-4869.
42. K. B. Sagomonyants, M. L. Jarman-Smith, J. N. Devine, M. S. Aronow and G. A. Gronowicz, *Biomaterials*, **2008**, 29, 1563-1572.
43. J. Dufils, F. Faverjon, C. Héau, C. Donnet, S. Benayoun and S. Valette, *Surface and Coatings Technology*, **2017**, 313, 96-106.
44. A. Escudeiro, M. Wimmer, T. Polcar and A. Cavaleiro, *Tribology International*, **2015**, 89, 97-104.
45. H. Wang, M. Xu, W. Zhang, D. T. Kwok, J. Jiang, Z. Wu and P. K. Chu, *Biomaterials*, **2010**, 31, 8181-8187.
46. K. Bazaka, M. Jacob, W. Chrzanowski and K. Ostrikov, *Rsc Advances*, **2015**, 5, 48739-48759.
47. K. Bazaka, M. V. Jacob and K. Ostrikov, *Chemical reviews*, **2015**, 116, 163-214.
48. A. Nourbakhsh, M. Cantoro, T. Vosch, G. Pourtois, F. Clemente, M. H. van der Veen, J. Hofkens, M. M. Heyns, S. De Gendt and B. F. Sels, *Nanotechnology*, **2010**, 21, 435203.
49. S. Peng, P. Feng, P. Wu, W. Huang, Y. Yang, W. Guo, C. Gao and C. Shuai, *Scientific reports*, **2017**, 7, 46604.
50. Y. Xu, W. Hong, H. Bai, C. Li and G. Shi, *Carbon*, **2009**, 47, 3538-3543.
51. W. Wu, P. Geng, J. Zhao, Y. Zhang, D. Rosen and H. Zhang, *Materials Research Innovations*, **2014**, 18, S5-12-S15-16.
52. M. I. D. B. Bouchet, J. M. Martin, J. Avila, M. Kano, K. Yoshida, T. Tsuruda, S. Bai, Y. Higuchi, N. Ozawa and M. Kubo, *Scientific Reports*, **2017**, 7, 46394.
53. I. Bertóti, M. Mohai and K. László, *Carbon*, **2015**, 84, 185-196.
54. M. Baraket, S. Walton, Z. Wei, E. Lock, J. Robinson and P. Sheehan, *Carbon*, **2010**, 48, 3382-3390.
55. O. Akhavan and E. Ghaderi, *ACS nano*, **2010**, 4, 5731-5736.
56. J. Li, G. Wang, H. Zhu, M. Zhang, X. Zheng, Z. Di, X. Liu and X. Wang, *Scientific reports*, **2014**, 4, 4359.
57. H. Zhao, S. Fan, Y. Chen, Z. Feng, H. Zhang, W. Pang, D. Zhang and M. Zhang, *ACS applied materials & interfaces*, **2017**, 9, 40774-40781.
58. J. Chen, X. Shi, S. Qi, M. Mohai, I. Bertóti, Y. Gao and H. Dong, *Carbon*, **2015**, 95, 338-346.